

# Quantum stability of self-organized atomic insulator-like states in optical resonators

Jonas Larson,<sup>1</sup> Sonia Fernández-Vidal,<sup>1,2</sup> Giovanna Morigi,<sup>2</sup> and Maciej Lewenstein<sup>3,4</sup>

<sup>1</sup>*ICFO-Institut de Ciències Fotòniques, E-08860 Castelldefels, Barcelona, Spain*

<sup>2</sup>*Departament de Física, Universitat Autònoma de Barcelona, E-08193 Bellaterra, Spain*

<sup>3</sup>*ICREA and ICFO-Institut de Ciències Fotòniques, E-08860 Castelldefels, Barcelona, Spain*

<sup>4</sup>*Institut für Theoretische Physik, Universität Hannover, D-30167 Hannover, Germany*

(Dated: June 21, 2024)

We investigate a paradigm example of cavity quantum electrodynamics with many body systems: an ultracold atomic gas inside a pumped optical resonator. In particular, we study the stability of atomic insulator-like states, confined by the mechanical potential emerging from the cavity field spatial mode structure. As in open space, when the optical potential is sufficiently deep, the atomic gas is in the Mott-like state. Inside the cavity, however, the potential depends on the atomic distribution, which determines the refractive index of the medium, thus altering the intracavity field amplitude. We derive the effective Bose-Hubbard model describing the physics of the system in one dimension and study the crossover between the superfluid – Mott insulator quantum states. We determine the regions of parameters where the atomic insulator states are stable, and predict the existence of overlapping stability regions corresponding to competing insulator-like states. Bistable behavior, controlled by the pump intensity, is encountered in the vicinity of the shifted cavity resonance.

PACS numbers: 03.75.Hh, 05.30.Jp, 32.80.Qk, 42.50.Vk

## I. INTRODUCTION

Cavity Quantum Electrodynamics (CQED) [1, 2] has been a key area of quantum optics in the last decades. In its early days one of its main focus was on optical instabilities, such as optical bistability [3], where the non-linear regime of the coupling between atoms and the modes of an optical resonator was achieved via the collective response of the atomic gas. In this regime, both cavity field and atomic degrees of freedom are well described "semi-classically" by macroscopic collective variables, while quantum fluctuations play a limited role. A drastically different situation has been achieved with high-finesse resonators, where the strong-coupling regime can be reached at the level of single atoms interacting with a single photon [4, 5, 6, 7, 8, 9]. In this regime, quantum electrodynamic effects are dominant.

In the recent years considerable attention has been paid to a new regime of CQED, which we term *CQED with many-body systems*. These studies focus onto the mechanical effects of the resonator field on the atomic motion, and on the nonlinearity arising from the interdependence between the cavity field, which depends on the atomic position, and the atomic motion, which is determined by the mechanical potential resulting from the spatial gradient of the cavity field mode. Following the theoretical prediction of Ref. [11], signatures of self-organization have been measured in the light scattered by laser-cooled atoms in a transversally-pumped cavities [10]. These structures have been theoretically studied in detail in Ref. [12], and the properties of the scattered light have been investigated in [13]. In different setups, Bragg scattering of atomic structures inside optical resonators has been experimentally investigated in [14]. While in all these cases the atomic motion is essentially

classical, the stability of these structures in the quantum regime is still unexplored. This question acquires a special relevance in view of the recent experimental progress. In fact, strong atom-field coupling between Bose-Einstein condensed atoms (BEC) and the mode of a high-finesse optical cavity has been realized in the experiments reported in Refs. [15, 16]. It is also worth mentioning several proposals to employ CQED techniques for detection and manipulations of ultracold gases [17, 18, 19, 20].

The main idea behind CQED with many-body systems is to combine CQED with the many-body physics of ultracold atomic gases. In particular, ultracold atomic gases in optical lattices offer the unprecedented and unique possibility to study numerous paradigmatic systems of quantum many-body physics [21, 22]. These systems allow one to realize various versions of Hubbard models [23], a prominent example of which is the Bose-Hubbard model [24], which exhibits the superfluid (SF) – Mott insulator (MI) quantum phase transition [25]. The realization of the Bose-Hubbard model with ultracold atoms has been proposed in the seminal theoretical work by [26], and demonstrated in the milestone experiments of [27]. A still largely unexplored question is how these dynamics are modified inside a resonator, when the optical lattice is the cavity field, whose intensity is not varied independently but is critically determined by the atomic distribution inside the resonator.

In the recent work [28] we have applied and studied the Bose-Hubbard model for atoms in the one-dimensional potential of an optical resonator, extending the derivation first presented by Maschler and Ritsch in Ref. [29] and then applied in Refs. [30]. Let us shortly summarize the main novel aspects of our model. The system we consider consists of ultracold atoms inside a resonator, which is driven by a laser. Due to the strong coupling between

cavity and atomic degrees of freedom, the field inside the cavity depends critically on the atomic distribution: In fact, the atoms shift the cavity resonance, thus modifying the intracavity field intensity. This in turn determines the depth of the cavity potential. At ultralow temperatures we may assume that atoms occupy only states of the lowest band of the periodic optical potential. Assuming the tight-binding regime, we may describe these states using Wannier functions [31], whose form is determined by the optical potential. Note, however, that the potential depends on the Wannier functions themselves. The problem is hence highly non-linear, as Wannier functions depend functionally on some integrals of Wannier functions, and have to be determined self-consistently.

In this article we report the details of the derivations presented in [28], and we extend our derivation to novel regimes. We focus on the SF-MI crossovers for a gas of few hundred atoms trapped by the potential of an optical resonator. We determine the boundaries of the MI states, evaluating the dependence of the chemical potential  $\mu$  on the parameters of the system: number of atoms  $N$ , pump strength and frequency. In order to calculate the boundaries of the MI states, we apply the *strong coupling expansion* of Ref. [32], which is one of the most accurate methods for the calculation of the phase-diagram of the one-dimensional BH model [22]. In our system, the coefficients of the Hubbard model depend on the number of atoms  $N$ . As a consequence, the diagrams in the  $\mu$ - $t$  plane, where  $t$  is the tunneling energy, exhibit overlapping, competing Mott states, that may even consist of disconnected regions for a wide range of parameters. In the vicinity of the shifted cavity resonance in the strong coupling regime the situation is even more complex: one encounters there also dispersive bistable behavior [3]; consequently, even for fixed  $N$  the Wannier functions can attain different forms. Thus, from the quantum optical perspective, this paper studies stability of Mott-like phases, i.e. insulator-like in an optical resonator.

This article is organized as follows. In Sec. II we present our model that describes a system of two level atoms confined in the two transverse direction and contained inside an optical cavity. In Sec. II A we introduce the single-atom Hamiltonian. The many-body dynamics involving the cavity damping is introduced in Sec. II B. Section II C is devoted to the physical discussion of the role of the various physical parameters on the system dynamics. The effective Bose-Hubbard Hamiltonian is derived in Sec. III, where the self-consistent Wannier functions are introduced and the final form the effective BH Hamiltonian is presented. In Sec. IV we discuss the ground-state properties of our model. We use the Gaussian approximation for the Wannier wave functions, checking carefully its validity. Within the Gaussian approximation and the strong coupling expansion method of H. Monien [32] the stability regions for the Mott states are obtained analytically, up to the solution of the non-linear self-consistent equation for the width of

the Wannier functions. Numerical results are reported and their physical meaning is discussed in Sec. IV B, while the validity of approximations is addressed once more in Sec. IV C. We conclude in Sec. V, while in the appendices the details of the derivation of the effective Hamiltonian and of the strong coupling expansion method are reported.

## II. THE MODEL

In this section we generalize the quantum optical model of a single atom inside a cavity to the many-body case, considering particle collisions at ultralow temperatures and quantum statistics. At this purpose, we first introduce the single-atom dynamics, write then the Hamiltonian in second quantization, introducing atom-atom collisions, and discuss the basic properties.

### A. Single-particle dynamics

We consider a single atom of mass  $M$  inside a cavity. The atomic dipole transition at frequency  $\omega_0$ , between the ground state  $|g\rangle$  and the excited state  $|e\rangle$ , couples quasi-resonantly with an optical mode of the resonator at frequency  $\omega_c$ , wave vector  $k$  and position-dependent coupling strength

$$g(x) = g_0 \cos(kx),$$

$g_0$  being the vacuum Rabi frequency. The resonator is driven by a classical field of amplitude  $\eta$  and oscillating at frequency  $\omega_p$ . We consider the atomic motion along the cavity axis, which coincides here with the  $x$ -axis, and assume tight confinement along the radial plane so that the radial motion can be considered frozen out. Atomic center-of-mass position and momentum operators are  $x$  and  $p$ , fulfilling the uncertainty relation  $[x, p] = i\hbar$ . In the reference frame oscillating at the frequency  $\omega_p$  of the pump field, the normally-ordered Hamiltonian describing the coherent dynamics of the atomic and cavity mode state reads

$$H_{JC} = \frac{p^2}{2m} - \hbar\Delta_a\sigma^\dagger\sigma - \hbar\Delta_c a^\dagger a - i\hbar g_0 \cos(x) (\sigma^\dagger a - a^\dagger \sigma) - i\hbar\eta (a - a^\dagger), \quad (1)$$

where  $\Delta_a = \omega_p - \omega_a$  and  $\Delta_c = \omega_p - \omega_c$  are the pump-atom and pump-cavity detunings,  $a$  ( $a^\dagger$ ) the annihilation (creation) operator of a cavity photon at frequency  $\omega_c$ , fulfilling the commutation relation  $[a, a^\dagger] = 1$ , and  $\sigma = |g\rangle\langle e|$ ,  $\sigma^\dagger = |e\rangle\langle g|$  the dipole lowering and raising operators. Spontaneous emission of the atomic dipole at rate  $\gamma$  and cavity losses at rate  $\kappa$  are described within the quantum Langevin equations formalism, such that the quantum Heisenberg-Langevin equations for the dipole and cavity

operators read [1]

$$\dot{a}(t) = (i\Delta_c - \kappa)a(t) + g(x)\sigma(t) + \eta + \sqrt{2\kappa}a^{in}(t) \quad (2)$$

$$\dot{\sigma}(t) = \left[ i\Delta_a - \frac{\gamma}{2} \right] \sigma(t) + g(x)\sigma_z a + \sqrt{\gamma}\sigma_z f^{in}(t) \quad (3)$$

$$\begin{aligned} \dot{\sigma}_z(t) = & 2g(x) [\sigma^\dagger a + a^\dagger \sigma] - \gamma (\sigma_z(t) + 1) / 2 \\ & + 2\sqrt{\gamma} (\sigma^\dagger f^{in} + f^{in\dagger} \sigma), \end{aligned} \quad (4)$$

where  $\sigma_z = \sigma^\dagger \sigma - \sigma \sigma^\dagger$  and  $a^{in}, f^{in}$  are the input noise operators, whose mean value vanishes and which are  $\delta$ -correlated in time, namely

$$\langle a^{in}(t) a^{in\dagger}(t') \rangle = \delta(t - t'), \quad (5)$$

$$\langle f^{in}(t) f^{in\dagger}(t') \rangle = \delta(t - t'). \quad (6)$$

At large atom-pump detuning the adiabatic elimination of the excited atomic state can be performed. Assuming that the changes in the atomic position are negligible during the time scale in which the atom reaches its internal steady state, namely when  $k_B T \ll \hbar|\Delta_a|$ , we solve the Heisenberg-Langevin equations at a fixed value of the atomic position  $x$ . Hence, for  $|\Delta_a| \gg g_0\sqrt{\langle n \rangle}, \gamma, |\Delta_c|$ , we set  $\sigma_z(t) \approx -1$  in the equations, and obtain  $\sigma^\dagger \approx ig(x)a^\dagger/\Delta_a$ . After tracing out the internal degrees of freedom, the single-particle Hamiltonian for cavity and atomic center-of-mass degrees of freedom reads

$$H_0 = \frac{\hat{p}^2}{2m} + \hbar [U_0 \cos^2(k\hat{x}) - \Delta_c] \hat{a}^\dagger \hat{a} - i\hbar\eta (\hat{a} - \hat{a}^\dagger), \quad (7)$$

where we have used the explicit form of the cavity spatial mode function, and

$$U_0 = g_0^2/\Delta_a \quad (8)$$

is the depth of the single-photon dipole potential.

## B. Many-body dynamics

We now extend the previous model and derive the corresponding effective Hamiltonian for a gas of  $N$  bosons at ultralow temperatures. The particle interactions are modeled by  $s$ -wave scattering. We introduce the field operators  $\Psi_j(x), \Psi_j^\dagger(x)$ , with  $j = g, e$  labeling the internal ground state, such that

$$[\Psi_j(x), \Psi_i^\dagger(x')] = \delta_{ij} \delta(x - x') \quad (9)$$

$$[\Psi_j(x), \Psi_i(x')] = [\Psi_j^\dagger(x), \Psi_i^\dagger(x')] = 0. \quad (10)$$

In second quantization the Hamiltonian (1) becomes  $\mathcal{H}$  and is decomposed according to  $\mathcal{H} = \mathcal{H}_0 + \mathcal{H}_1$ , where

$$\mathcal{H}_0 = \sum_{j=g,e} \int dx \Psi_j^\dagger(x) \left( -\frac{\hbar^2 \nabla^2}{2m} + \frac{1}{2} u_j \Psi_j^\dagger(x) \Psi_j(x) \right) \Psi_j(x) \quad (11)$$

with  $u_j$  the strength of the onsite interaction depending on the atomic state, and

$$\begin{aligned} \mathcal{H}_1 = & -\hbar\Delta_a \int dx \Psi_e^\dagger(x) \Psi_e(x) - \hbar\Delta_c a^\dagger a - i\hbar\eta (a - a^\dagger) \\ & - i\hbar g_0 \int dx \cos(kx) [\Psi_e^\dagger(x) \Psi_g(x) a - a^\dagger \Psi_g^\dagger(x) \Psi_e(x)]. \end{aligned} \quad (12)$$

In the above description we omit to write the Hamiltonian term describing the collisions between atoms in different internal states, as we will consider that the excited state is essentially empty in the parameter regime we choose. The quantum Heisenberg-Langevin equations for atomic and field operators read

$$\begin{aligned} \dot{\Psi}_g(x) = & -\frac{i}{\hbar} [\Psi_g(x), \mathcal{H}_0] \\ & + g_0 \cos(kx) a^\dagger \Psi_e(x) - \sqrt{\gamma} f^{in\dagger} \Psi_e(x) \end{aligned} \quad (13)$$

$$\begin{aligned} \dot{\Psi}_e(x) = & -\frac{i}{\hbar} [\Psi_e(x), \mathcal{H}_0] + i\Delta_a \Psi_e(x) \\ & - g_0 \cos(kx) \Psi_g(x) a - \frac{\gamma}{2} \Psi_e(x) + \sqrt{\gamma} \Psi_g(x) f^{in} \end{aligned} \quad (14)$$

$$\begin{aligned} \dot{a} = & (i\Delta_c - \kappa)a + \eta + \sqrt{2\kappa} a_{in} \\ & + g_0 \int dx \cos(kx) \Psi_g^\dagger(x) \Psi_e(x), \end{aligned} \quad (15)$$

where  $f^{in}(t)$  and  $a_{in}(t)$  are the noise operators defined in the previous section. Solving the equation for  $\Psi_e(x, t)$  in the limit of large detuning,  $|\Delta_a| \gg \gamma, g_0\sqrt{\langle n \rangle}$ , we find

$$\Psi_e(x) \sim -i \frac{g_0 \cos(kx)}{\Delta_a} \Psi_g(x) a, \quad (16)$$

where the adiabatic approximation lies on the assumption that  $\hbar|\Delta_a| \gg k_B T$ , as in the single-particle case, and we have neglected the input noise term, assuming the decay rate  $\gamma \ll |\Delta|$ . Substituting this value into Eq. (15), the Heisenberg-Langevin equation for the field is given by

$$\dot{a} = (i\Delta_c - \kappa)a + \eta + \sqrt{2\kappa} a_{in} - iU_0 \mathcal{Y} a,$$

where

$$\mathcal{Y} = \int dx \cos^2(kx) \Psi_g^\dagger(x) \Psi_g(x) \quad (17)$$

is the integral of the density of atoms in the electronic ground state, weighted by the cavity spatial mode function. We now assume the bad-cavity limit, namely the cavity field relaxes to the steady state on a much faster time scale than the one in which the atomic medium varies. This limit implies  $\kappa \gg k_B T/\hbar$ , and consistency with the previous assumption imposes  $|\Delta_a| \gg \kappa \gg k_B T/\hbar$ . In this limit the dependence of the field on the initial condition is negligible, and its solution is essentially the inhomogeneous one that can be written as

$$a \simeq \eta F(\mathcal{Y}). \quad (18)$$

Here we have discarded the input noise term, as we are dealing with normally-ordered equations, and introduced the operator

$$F(\mathcal{Y}) = \frac{1}{\kappa - i(\Delta_c - U_0\mathcal{Y})}, \quad (19)$$

which is a function of the atom operators in the ground state. Substituting into the equation for the ground-state field operator we obtain

$$\dot{\Psi}_g = -\frac{i}{\hbar}[\Psi_g(x), \mathcal{H}_0] - i\mathcal{C}(\mathcal{Y}, x), \quad (20)$$

where

$$\mathcal{C}(\mathcal{Y}, x) = \eta^2 U_0 \cos^2(kx) F^\dagger(\mathcal{Y}) \Psi_g(x) F(\mathcal{Y}). \quad (21)$$

### C. Discussion

Equation (20) shows explicitly the effect of the coupling with the resonator on the atom dynamics: The coupling to the common cavity mode induces a non-linear interaction, which enters in the equation through operator (19). It is useful to consider the average number of photons at steady state  $n_{\text{ph}} = \langle a^\dagger a \rangle_{\text{St}}$ , which we obtain from Eq. (18) and reads

$$n_{\text{ph}} = \left\langle \frac{\eta^2}{\kappa^2 + (\Delta_c - U_0\mathcal{Y})^2} \right\rangle. \quad (22)$$

The average number of photons  $n_{\text{ph}}$  hence depends on the atomic density distribution. On the other hand, it determines the depth of the confining potential,  $V \approx \hbar|U_0|n_{\text{ph}}$ , and thus the atomic density distribution. In particular, the confining potential reaches a maximum for the values at which the denominator of Eq. (22) is minimum. From the form of operator (18) one infers that  $n_{\text{ph}}$  can reach the maximum value when parameters  $\Delta_c$  and  $U_0$  have the same sign (the operator  $\mathcal{Y}$  is positive valued). From Eq. (8) this requires that detunings  $\Delta_c$  and  $\Delta_a$  have equal signs. This property highlights the role of the detuning in the dynamics as control parameters.

We now comment on the parameters required for accessing the regime in which the effect of the non-linearity will be important, and its consistency with the derivation we performed. The non-linear dependence of the potential on the atomic density distribution will be relevant when the values assumed by operator  $U_0\mathcal{Y}$  in (18) is of the order of, or even larger than, the cavity linewidth  $\kappa$ . Let us assume that  $|U_0| \sim \kappa$ . Our derivation is based on the important assumption that spontaneous decay is negligible, which leads to the inequality

$$\gamma \frac{g_0^2 n_{\text{ph}}}{\Delta_a^2} \ll \kappa.$$

That is, the only source of noise is cavity decay for sufficiently long times. This inequality is consistent with

the requirement on  $U_0$  when  $\gamma n_{\text{ph}}/|\Delta_a| \ll 1$ . Taking the maximum for the photon number,  $n_{\text{ph}} \sim \eta^2/\kappa^2$ , we find

$$\frac{\gamma}{|\Delta_a|} \frac{\eta^2}{\kappa^2} \ll 1.$$

For  $n_{\text{ph}} \sim 100$ , this gives  $|\Delta| \sim 10^3\gamma$ . The parameter regime  $U_0 \simeq \kappa$  requires high-finesse resonators, with  $g_0 \sim \sqrt{|\Delta_a|\kappa}$ .

## III. THE BOSE-HUBBARD HAMILTONIAN

### A. Derivation of the Bose-Hubbard Model

We now derive a Bose-Hubbard type of model for the dynamics of the atoms in their self-sustained potential when the atoms are well localized in the minima of the potential itself. Starting from the assumption that the atoms are in a Mott-insulator state, we decompose the atomic field operator into the operators  $b_i^\dagger, b_i$ , which create, respectively annihilate, atoms at the lowest band of the potential site centered at  $x = x_i$ , according to

$$\hat{\Psi}(x) = \sum_i \tilde{w}(x - x_i) \hat{b}_i, \quad (23)$$

whereby  $\tilde{w}(x - x_i)$  are Wannier functions, which are to be determined by solving self-consistently the equations of motion. The commutation rules of operators  $b_i, b_i^\dagger$  obey the bosonic commutation relations in the regular Bose-Hubbard model, where the potential is independent of the state of the atoms. We will show that in our case this is not *a priori* warranted, due to the non-linear dependence of the potential on the atomic density distribution, which gives rise to a non-linear equation for the atomic wave function. However, the bosonic commutation relations are still recovered in a properly defined thermodynamic limit, which we will identify.

We rewrite now Eq. (20) within this Wannier decomposition,

$$\dot{b}_\ell = \frac{1}{i\hbar}[b_\ell, \mathcal{H}_0^{(BH)}] - iC, \quad (24)$$

where  $\mathcal{H}_0^{(BH)}$  and  $C$  are obtained from  $\mathcal{H}_0$  and  $\mathcal{C}$ , respectively, using the Bose-Hubbard decomposition. They read

$$\mathcal{H}_0^{(BH)} = E_0 \hat{N} + E_1 \hat{B} + \frac{U}{2} \sum_i b_i^\dagger b_i^\dagger b_i b_i - \mu \hat{N}, \quad (25)$$

and

$$C = U_0 \eta^2 F^\dagger(\hat{Y}) [J_0 b_\ell + J_1 (b_{\ell+1} + b_{\ell-1})] F(\hat{Y}). \quad (26)$$

The coupling matrix elements in Eqs. (25)-(26) read

$$E_l = -\frac{\hbar^2}{2m} \int dx \tilde{w}(x-x_i)^* \nabla^2 \tilde{w}(x-x_{i+l}) \quad (27)$$

$$J_l = \int dx \tilde{w}(x-x_i)^* \cos^2(kx) \tilde{w}(x-x_{i+l}) \quad (28)$$

$$U = u_g \int dx |\tilde{w}(x)|^4 \quad (29)$$

and with  $l = 0, 1$  we have only kept on-site and nearest-neighbour couplings. In Eq. (26) we introduced the operator

$$F(\hat{Y}) = \frac{1}{\kappa - i(\Delta_c - U_0 \hat{Y})}, \quad (30)$$

where operator  $\hat{Y}$  is the Bose-Hubbard decomposition of  $\mathcal{Y}$ , Eq. (17), after neglecting couplings beyond the nearest neighbors, and takes the form  $\hat{Y} = J_0 \hat{N} + J_1 \hat{B}$ .

In order to determine the Bose-Hubbard Hamiltonian, we now derive an effective Hamiltonian  $\mathcal{H}_{BH}$  such that  $C = [b_\ell, \mathcal{H}_{BH}]/\hbar$ . This is performed in the limit in which we can expand operator  $F$  in Eq. (30) in the small quantity  $J_1$ . The details of the derivation are reported in App. A. The Bose-Hubbard model is recovered for a large number of atoms, according to a properly defined thermodynamic limit. We define the thermodynamic limit taking the scaling  $U_0 \sim 1/N$ , and  $\eta \sim \sqrt{N}$ , which corresponds to keeping the potential depth constant as  $N$  increases. This scaling corresponds to ramping up the pump intensity with  $\sqrt{N}$  and scaling the atomic detuning  $\Delta_a$  linearly with the number of particles [33]. The Bose-Hubbard type of Hamiltonian  $\mathcal{H}_{\text{eff}} = \mathcal{H}_0^{(BH)} + \mathcal{H}_{BH}$  is then

$$\mathcal{H}_{\text{eff}} = E_0 \hat{N} + \frac{U}{2} \sum_i \hat{n}_i (\hat{n}_i - 1) - t(\hat{N}) B + f(\hat{N}) - \mu \hat{N}, \quad (31)$$

where

$$t(\hat{N}) = -E_1 - \hbar \eta^2 U_0 J_1 F^\dagger(J_0 \hat{N}) F(J_0 \hat{N}) \quad (32)$$

$$f(\hat{N}) = \frac{\hbar \eta^2}{\kappa} \arctan \left( \frac{\Delta_c - U_0 J_0 \hat{N}}{\kappa} \right). \quad (33)$$

We notice that the coefficients of Hamiltonian (31) are operator-valued, hence imposing a Wannier expansion such that the coefficients depend on the operator  $\hat{N}$ , namely

$$\tilde{w}(x-x_i) = w(\hat{N}, x-x_i).$$

Hence, the commutation relations between the operators  $b_i$  are not the ones of bosonic operators as in the typical Bose-Hubbard model. Nevertheless, in the thermodynamic limit we identified one finds

$$[b_i, b_j^\dagger] = \delta_{ij} + \mathcal{O}(1/N). \quad (34)$$

We therefore perform the Wannier expansion in this thermodynamic limit, consistently with the assumptions made in order to obtain the Hamiltonian (31).

## B. The Bose-Hubbard Hamiltonian

We rescale now Hamiltonian (31) and obtain the Hamiltonian  $\hat{H} = \hat{H}/U$ , where  $U$  is the strength of the on-site interaction defined in eq. (29) and

$$\hat{H} = -\tilde{t} \hat{B} + \frac{1}{2} \sum_i \hat{n}_i (\hat{n}_i - 1) - \tilde{\mu} \hat{N}, \quad (35)$$

where

$$\tilde{\mu} = \frac{\mu + E_0}{U} + \frac{f(\hat{N})}{\hat{N}U} \quad (36)$$

contains a rescaled chemical potential, while the tunnel parameter

$$\tilde{t} = -\frac{E_1}{U} - \frac{\hbar \eta^2 U_0 J_1}{U(\kappa^2 + \zeta^2)} \quad (37)$$

is expressed in terms of a coefficient

$$\zeta = \Delta_c - U_0 J_0 \hat{N}. \quad (38)$$

The higher order terms in  $J_1 \hat{B}$ , describing long-range interaction, have been neglected. Note that the number of particles is conserved since  $[\hat{N}, \hat{H}] = 0$ . We also remark that the term  $f(N)/N$  tends to a constant and finite value in the thermodynamic limit.

An important physical quantity, which will be useful for the following study, is the depth  $V$  of the cavity potential,  $\tilde{V}(x) = V \cos^2 kx$ , with  $V = \hbar U_0 n_{\text{ph}}$ . Here  $n_{\text{ph}}$  is the number of photons in the Bose-Hubbard expansion, Eq. (22), and which takes the form

$$V = \frac{\eta^2 \hbar U_0}{\kappa^2 + \zeta^2} \quad (39)$$

at leading order in the expansion in  $J_1$ . Hamiltonian (35) and potential (39) are the starting points of our analysis for the determination of the system's ground-state.

Let us now make some considerations about the system for a fixed number of atoms  $N$ . From the form of the potential (39), and in particular from the form of the coefficient  $\zeta$ , Eq. (38), we observe that for equal signs of the detunings  $\Delta_a$  and  $\Delta_c$  one can have that  $\zeta$  vanishes. This case corresponds to driving the system on resonance, and gives a maximum of the cavity mode potential. This resonance situation occurs for atom numbers  $N$  that maximize the photon number, and gives rise to bistability, which modifies substantially the properties of the model with respect to this Bose-Hubbard one.

## IV. DETERMINATION OF THE GROUND-STATE

In this section we determine the ground-state of the system for a fixed number of particles. Moreover, we

discuss the situation when the number of atoms is fluctuating. Our purpose is to identify the parameter regime in which the atoms are in the Mott-insulator state.

Starting from the assumption that the system is in the Mott-insulator state, we use the *strong coupling expansion* [32] to verify its validity. In particular, we apply a standard degenerate-perturbation calculation in the parameter  $\tilde{t} = t/U$ , and determine the ground-state energy  $E_M(n_0, \tilde{\mu}, \tilde{t})$  for the Mott state with  $n_0$  particles per site, and the ground-state energies  $E_{\pm}(n_0, \tilde{\mu}, \tilde{t})$  when one particle is added or subtracted to the  $n_0$ th Mott state. The condition

$$E_M(n_0, \tilde{\mu}, \tilde{t}) - E_{\pm}(n_0, \tilde{\mu}, \tilde{t}) = 0 \quad (40)$$

determines the boundaries  $\tilde{\mu}_{\pm}(n_0)$  of the  $n_0$ th Mott phase as a function of the coupling parameter. For  $\tilde{\mu}_+(n_0) > \tilde{\mu}_-(n_0)$  the region between the two chemical potentials determines the Mott zone. The Mott state gets unstable as the parameters are varied such that  $\tilde{\mu}_+(n_0) = \tilde{\mu}_-(n_0)$  and finally  $\tilde{\mu}_+(n_0) < \tilde{\mu}_-(n_0)$ . In this section we determine the boundaries of the Mott state in a diagram, in which we plot  $\tilde{\mu}$  as a function of relevant parameters. We remark that, in the typical Bose-Hubbard model, when the system exits the Mott phase, then it is in a superfluid state. In our case, this is probably verified in most cases, which we will discuss individually.

Finally, the parameter  $\tilde{t}$  can be varied by varying the pump amplitude  $\eta$ , which is straightforwardly related to the number of photons inside the cavity and hence to the height of the potential, or by varying the atom-pump detuning  $\Delta_a$  and the cavity-pump detuning  $\Delta_c$ , which enter in the dynamics through the denominator (38) and correspond to changing the refractive index of the atomic medium.

In the following we first study the functional dependence of the integrals on the system's parameters, using the Gaussian ansatz. We then determine numerically the regions of the Mott-insulator state in the diagram where the chemical potential  $\tilde{\mu}$  is studied as a function of the pump intensity  $\eta$ .

### A. Coefficients in the Gaussian approximation

We determine analytically the boundaries of the Bose-Hubbard model using the *Gaussian approximation*, hence replacing the Wannier functions by Gaussian functions in the integrals (27)-(29). Thus, we approximate the Wannier functions with Gaussian functions such that

$$\tilde{w}(x - x_i) \approx \tilde{w}_G(x - x_i) \equiv (\pi\sigma^2)^{-1/4} e^{-\frac{(x-x_i)^2}{2\sigma^2}}, \quad (41)$$

where  $\sigma$  is the width to be determined. This treatment allows us to identify the dependence of the coefficients on the physical parameters, reproducing with good approximation the results obtained with the Wannier functions in the parameter regimes we discuss in Sec. IV C. We

modify the Gaussian functions in order to fulfill the orthogonality condition,  $\int \tilde{w}_G(x - x_i) \tilde{w}_G(x - x_j) dx = \delta_{ij}$ . In this way we avoid small, but unphysical contributions.

Let  $K$  be the number of lattice sites. The width  $\sigma$  of the Gaussian functions is found from the potential  $V$  of the cavity mode, Eq. (39). In particular,  $\sigma^2 = \hbar/\sqrt{2m|V|}k$ . In order to determine the boundaries of the Mott states in the diagram of  $\tilde{\mu}$  as a function of  $\eta$ , we determine the coefficients for the three cases (1)  $N = Kn_0 + 1$ , (2)  $N = Kn_0$  and (3)  $N = Kn_0 - 1$ , and introduce the subscript  $(i)$  with  $i = 1, 2, 3$  for the corresponding coefficient. We evaluate the integrals in Eqs. (27)-(29) for these three cases and express them as a function of the dimensionless parameter

$$y_{(i)} = k^2\sigma_{(i)}^2 = \sqrt{E_R/|V_{(i)}|}, \quad (42)$$

where  $E_R$  is the recoil energy. In terms of  $y_{(i)}$ , they read

$$E_{0(i)} = \frac{E_R}{2y_{(i)}}, \quad (43)$$

$$J_{0(i)}^{\pm} = \frac{1}{2} [1 - \text{sign}(\Delta_a) \exp(-y_{(i)})], \quad (44)$$

$$E_{1(i)} = -\frac{|V_{(i)}|}{4} \exp\left(-\frac{\pi^2}{4y_{(i)}}\right) (2y_{(i)} + \pi^2), \quad (45)$$

$$J_{1(i)}^{\pm} = \frac{\text{sign}(\Delta_a)}{2} \exp\left(-\frac{\pi^2}{4y_{(i)}} - y_{(i)}\right), \quad (46)$$

$$U_{(i)} = \frac{4E_R a_s}{\sqrt{2\pi}\Delta_{yz}} y_{(i)}, \quad (47)$$

where  $a_s$  is the scattering length,  $\Delta_{yz}$  is the atomic wave packet transverse width and the  $\pm$ -sign comes from the sign of  $\Delta_a$ . In the limit  $J_{0(i)}^{\pm} \gg |J_{1(i)}^{\pm}|$  the potential amplitude according to (39) is given by

$$V_{(i)} = \frac{\eta^2 \hbar U_0}{\kappa^2 + \left(\Delta_c - U_0 J_{0(i)}^{\pm} N\right)^2}. \quad (48)$$

As  $J_{0(i)}^{\pm}$  depends on  $V_{(i)}$  which, on the other hand, depends itself on  $J_{0(i)}^{\pm}$ , the above equations must be solved self-consistently. This is a consequence of the atom-density dependence on the coupling parameters. In particular, for  $\Delta_a > 0$  (atoms at the nodes),  $J_{0(i)} = 0$  in the strong pumping limit and the results become independent of the number of atoms. On the other hand, if  $\Delta_a < 0$  (atoms at the antinodes) the parameter  $J_{0(i)} = 1$  for sufficiently large pumping, and the non-linearity is strongest.

Within this treatment we determine the nearest-neighbor coupling parameter, which is given by

$$\tilde{t}_{(i)} = \frac{E_R}{4\mathcal{U}} y_{(i)}^{-3/2} e^{-\frac{\pi^2}{4y_{(i)}}} (2y_{(i)} + \pi^2 - 2e^{-y_{(i)}}), \quad (49)$$

where  $\mathcal{U} = 2\hbar^2 a_s k / (\sqrt{2\pi} m \Delta_{yz})$ . For  $\eta \rightarrow \infty$  the potential  $|V_{(i)}| \rightarrow \infty$  and consequently  $y_{(i)} \rightarrow 0$ , and hence  $\tilde{t} \rightarrow 0$  [37].

The perturbative calculation of the boundaries  $\tilde{\mu}_{\pm}(n_0)$  is sketched in the appendix. In third order the result reads

$$\begin{aligned} \tilde{\mu}_{+}(n_0) &= n_0 + \frac{U_{(12)}}{2} K n_0 (n_0 - 1) - t_{(1)} 2(n_0 + 1) \\ &+ t_{(1)}^2 n_0^2 - \left( t_{(1)}^2 - t_{(2)}^2 \frac{U_{(2)}}{U_{(1)}} \right) 2K n_0 (n_0 + 1) \\ &+ t_{(1)}^3 n_0 (n_0 + 1) (n_0 + 2), \end{aligned} \quad (50)$$

$$\begin{aligned} \tilde{\mu}_{-}(n_0) &= (n_0 - 1) - \frac{U_{(32)}}{2} K n_0 (n_0 - 1) + t_{(3)} 2n_0 \\ &- t_{(3)}^2 (n_0 + 1)^2 + \left( t_{(3)}^2 - t_{(2)}^2 \frac{U_{(2)}}{U_{(3)}} \right) 2K n_0 (n_0 + 1) \\ &+ t_{(3)}^3 n_0 (n_0 + 1) (n_0 - 1). \end{aligned} \quad (51)$$

Here,  $U_{(i2)} = 1 - U_{(2)}/U_{(i)}$ ,  $\tilde{\mu}_{+}(n_0) = \mu_{+}(n_0)/U_{(1)}$  and  $\tilde{\mu}_{-}(n_0) = \mu_{-}(n_0)/U_{(3)}$ .

## B. Numerical results

In this section we study the regions of the Mott-insulator state in the diagram plotting the chemical potential as a function of the inverse pump amplitude  $\eta^{-1}$ . The boundaries are determined by numerical evaluation of Eqs. (27)-(29) using the Gaussian functions. We notice that the Gaussians at different lattice sites have non-vanishing overlaps, giving small, but nonetheless, non-physical contributions. One overcomes this problem by modifying the Gaussians as discussed in the previous section. The atomic parameters we choose correspond to  $^{87}\text{Rb}$  atoms with scattering length  $a_s = 5.77$  nm and atomic transition wavelength  $\lambda = 830$  nm. The cavity loss constant is  $\kappa = 2\pi \times 100$  kHz, the number of lattice sites  $K = 50$  and the transverse width of the atomic wave packet  $\Delta_y = \Delta_z = \sqrt{\Delta_{yz}} = 30$  nm. We analyse the stability of the Mott-insulator state for a fixed number of atoms and for different values of the detunings.

Figure 1 displays the first four Mott zones for (a)  $\Delta_a < 0$  and  $\Delta_c = \kappa$  and (b)  $\Delta_a > 0$  and  $\Delta_c = 0$ , as a function of the dimensionless parameter  $\kappa/\eta$ . Interestingly, the extension of the Mott zones seems to decrease roughly as  $n_0^{-1}$  in both cases. We first analyse the case displayed in Fig. 1(a). For  $\Delta_a < 0$  the atoms are trapped at the maxima of the intracavity field. Hence, the coupling with the cavity mode is maximum when the confinement is very tight,  $\eta \rightarrow \infty$ . Here, for large values of the pump intensity (i.e., for small values of  $\kappa/\eta$ ) the Mott zones at different values of  $n_0$  show some overlap. This overlap is a cavity QED effect, in fact Mott states with larger number of atoms per site are favored as they increase the coupling strength to the cavity mode, and thus the depth of the potential. The overlap is only at the border of the boundaries, as atom-atom collisions compete with this effect. In Fig. 1(b) the detuning  $\Delta_a > 0$ , and the atoms are hence trapped at the nodes (the zeroes) of the intracavity field. Hence, the coupling with the cavity

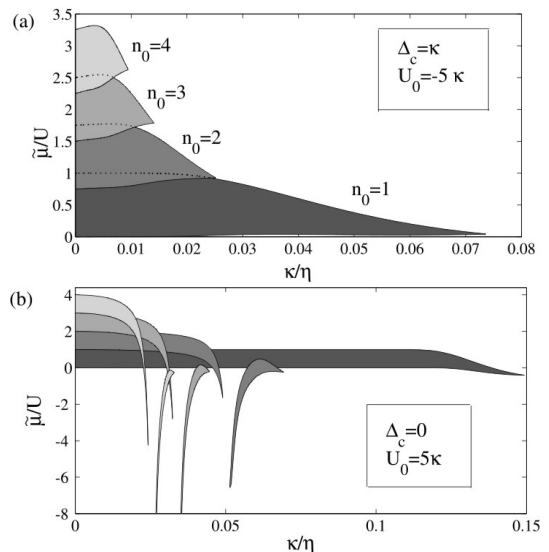


FIG. 1: The phase diagram where the Mott zones are plotted in the plane  $\tilde{\mu}-\eta^{-1}$  for (a)  $U_0 = -5\kappa$  ( $\Delta_a < 0$ , atoms at the antinodes),  $\Delta_c = 2\kappa$  and (b)  $U_0 = 5\kappa$  ( $\Delta_a > 0$ , atoms at the nodes),  $\Delta_c = 0$ . The dotted lines correspond to the boundaries of the covered Mott-zones.

mode is minimum when  $\eta \rightarrow \infty$ . Indeed, here we observe that for large values of  $\eta$  (small values of  $\kappa/\eta$ ), the Mott zones almost do not overlap. However, for smaller values of  $\eta$  they exhibit an "exotic" behavior: overlap, disappear and reappear.

Further insight is gained in Fig. 2, where we study the depth of the cavity potential as a function of the pump parameters. The curves displayed in Fig. 2(a) correspond to the parameters of the phase diagram in Fig. 1(a). Here, one observes that the potential amplitude increases monotonically as  $V \sim \eta^2$  in the parameter regime of the plot. Correspondingly, the width  $\sigma_{(i)}$  of the Wannier functions, giving atomic localization at the minima of the potential, decreases smoothly as  $\sigma_{(i)} \propto |V_{(i)}|^{-1/4} \sim 1/\sqrt{\eta}$ . The curves in Fig. 2(b) correspond to parameters of the phase diagram in Fig. 1(b). Here, one finds that the potential amplitude increases abruptly where the corresponding Mott zones exhibit a minimum in the value of  $\tilde{\mu}$ . Correspondingly, the width  $\sigma_{(i)} \propto |V_{(i)}|^{-1/4}$  diminishes rapidly. This behaviour changes at the value of  $\eta$  where the potential gradient increases abruptly. In this regime  $\sigma_i$  varies very slowly. This behavior can be understood as a competition between the cavity field, which tends to localize the atoms at the minima, and the atomic quantum fluctuations: When the potential is sufficiently high to trap the atoms within a small fraction of the wavelength, the cavity field is pumped more effectively.

We now consider the situation in which the detunings  $\Delta_a$  and  $\Delta_c$  have the same sign. In this case the parameter  $\zeta(N)$  in Eq. (38) vanishes when the condition  $J_{0(i)}^{\pm} = \Delta_c/U_0 N$  is fulfilled, whereby  $0 < J_{0(i)}^+ < 1/2$  and

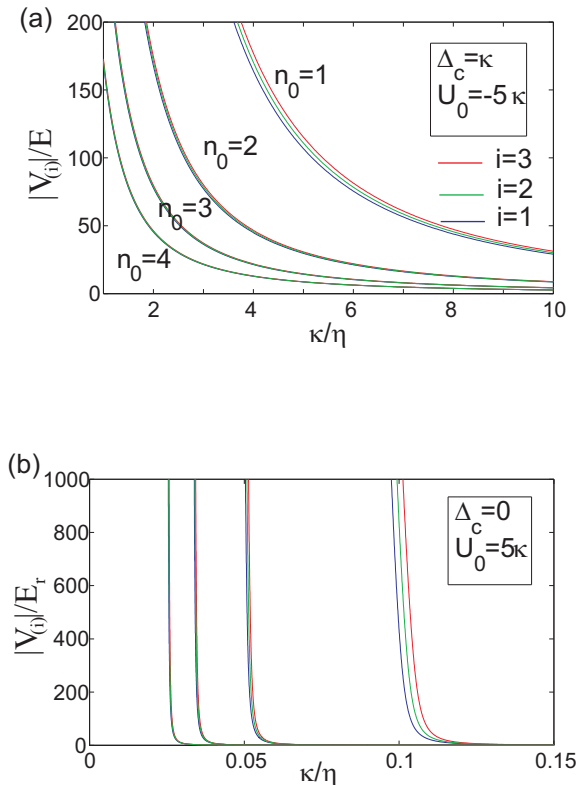


FIG. 2: (Colour online) The potential amplitude  $|V_{(i)}|$ , in units of  $E_r$ , as a function of the inverse pumping  $\kappa/\eta$  for (a) the parameter regime of fig 1 (a) and (b) of fig. 1 (b). The average number of cavity photons is found by multiplying the scaled amplitudes in the plots by the factor  $f_n = E_r/|\hbar U_0|$ , which here is  $f_n \approx 0.006$ .

$1/2 < J_{0(i)}^- < 1$ , see Eq. (44). This resonance condition gives rise to bistability, leading to an abrupt change of the potential height. As a consequence, the Mott state may become unstable. The upper plot of Fig. 3 displays the potential amplitudes  $V_{(i)}/E_r$  for one atom per site as function of  $\eta/\kappa$  for  $U_0 = -\kappa$  and  $\Delta_c = -45\kappa$ , exhibiting the typical functional behavior of bistability. The lower plot displays the corresponding phase diagram. For the case of one atom per site, the Mott ground-state will suddenly disappear for  $\eta \sim \kappa$  when the pumping is adiabatically lowered. Clearly the first "jump" occurs in the potential  $V_{(i)}$  (corresponding to the lowest atom density), and comparing the two plots one finds that this takes place exactly when the first Mott zone suddenly ends. The system most likely jumps into a state where higher Bloch bands are populated. In this case the single-band and Gaussian approximations break down.

The overlapping of the Mott zones and the bistability, which we observe in the phase diagram, are novel features

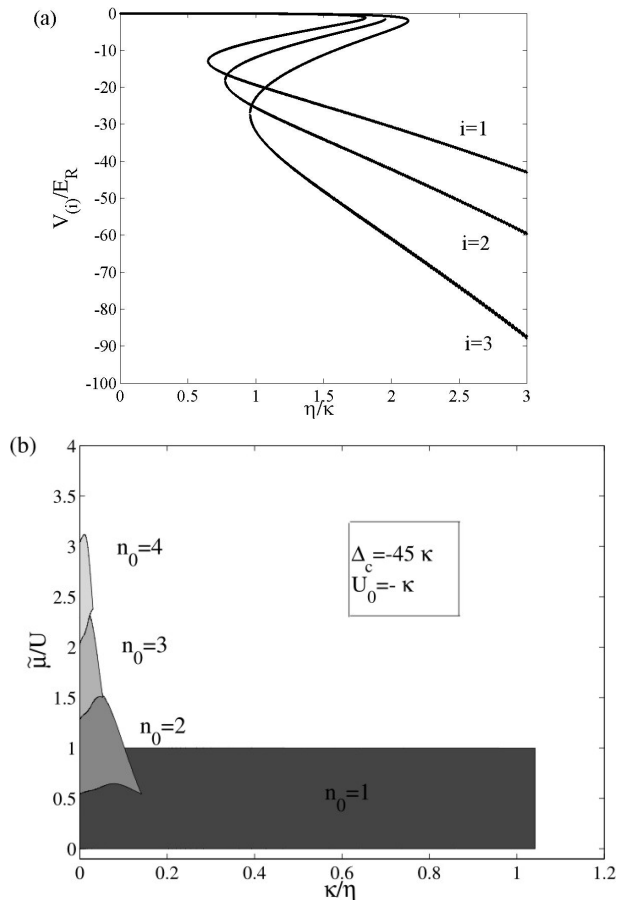


FIG. 3: Potential amplitudes  $V_{(i)}$  as a function of  $\kappa/\eta$  (upper plot) and phase diagram  $\tilde{\mu} - \eta^{-1}$  (lower plot) for  $\Delta_c = -45\kappa$ ,  $U_0 = -\kappa$ .

when compared with the typical scenario of cold atomic gases trapped by an external potential. Let us first discuss on the existence and uniqueness of the ground-state. When the Mott-insulator state is stable, given the number of atoms  $N$ , the ground state is fully determined once the atomic density  $\rho = N/K$  is fixed. Outside of the Mott zones we expect superfluidity in the parameter regimes in which there cannot be optical bistability (detunings with opposite signs). In the situation of multiple solutions of the Eqs. (43)-(47), the system will most likely be found in the one solution which minimizes the energy.

A more complete picture of the phase diagram can be obtained by considering the dependence on the atomic density. The strong coupling method for higher orders is cumbersome once the number of added/subtracted particles to the Mott states becomes larger than one. However, the first-order corrections are still easily obtainable for any atom number. In fig. 4 we present schematically the extended phase diagram of fig. 1 (a) where the atomic density has been included as a third axis. This diagram has been obtained by fitting the intermediate



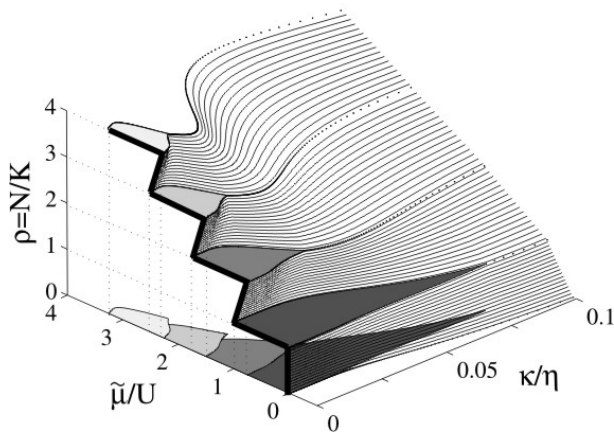


FIG. 4: Extended phase diagram of fig. 1 (a), where the atomic density  $\rho$  has been included as a third axis. Here, the contour lines correspond to a fixed atom density  $\rho$ , such that for a given  $\rho$  the scaled chemical potential depends on the pumping strength  $\eta$  according to this particular contour line. The dotted curves indicate the lines with exactly  $n_0$  atoms per site. The projection of the Mott-zones onto the  $\tilde{\mu} - \eta^{-1}$  plane is shown.

lines between the Mott zones, and by verifying that it reproduces the first order calculations for small values of  $\kappa/\eta$ . We remark that the "overhangs", corresponding to the overlapping zones in Fig. 1(a), constitute the novel feature, which we encounter in this model as compared to the standard Bose-Hubbard model.

When the number of atoms is not fixed [35], the atomic density may take multiple values where the phase diagram exhibits "overhangs". For sufficiently long times, we expect that the system will be found in the number of atoms such that the energy is minimized. This implies also that there may be a competition between a Mott and a superfluid state at two different values of the density, which happen to be at similar energies. Keeping this situation in mind, we restrict our analysis to different and overlapping Mott states, and compare their energy. Figure 5 displays a phase diagram on the  $\tilde{\mu} - \eta^{-1}$  plane, whereby the Mott states with higher energy are plotted on top of the ones with lower energy. We observe that for large pumping strengths the Mott states with a higher number of atoms  $n_0$  have in general a greater energy, while for lower or moderate pumping strengths this is not necessary true. For example, the end of the Mott zone with  $n_0 = 4$  has smaller energy than the corresponding one for the  $n_0 = 3$ . This is a pure CQED effect.

### C. Validity of the approximations

We now discuss the regime of validity of the calculations, from which we extracted the phase diagrams of this section.

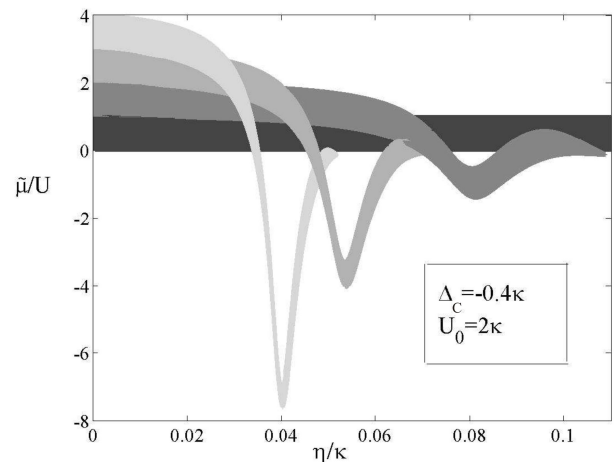


FIG. 5: Phase diagram on the  $\tilde{\mu} - \eta^{-1}$  plane, reporting the first four Mott zones. The Mott states with higher energy are plotted on top of the ones with lower energy.

The derivation of the system coupling parameters relies on the assumption  $J_0 \gg |J_1^\pm|$ . Since the maximum value of the ratio  $|J_1^\pm|/J_0 \approx 0.056$  occurs at  $|V| \approx E_r/2$ , hence the nearest-neighbor coupling is at least 17 times smaller than the on site coupling. The expansion to first order in  $J_1 B$  of Eq. (30) is motivated for any number of atoms since the perturbative parameter  $\lambda \equiv J_1 \hat{B}/J_0 \hat{N} \sim J_1/J_0$  is strictly smaller than unity.

The values of the chemical potential, as in Eq. (50), are derived from a third-order perturbation expansion in the parameter  $\tilde{t} = t/U$  and it is expected to break down for large  $\tilde{t}$ . We verified that in general  $\tilde{t} < 0.25$ . Moreover, we compared the phase diagrams with the ones obtained by truncating at the second order in  $\tilde{t}$ , and could verify that they do not differ substantially one from the others. We remark that the perturbation calculations are carried out assuming periodic boundary conditions, while the system here studied has a fixed number of sites,  $K = 50$ . We checked the validity of the assumption by comparing the results obtained for different lattice sites, up to 1000, keeping the density fixed.

As it concerns the tight-binding approximation (i.e., only including nearest neighbor couplings), the single-band approximation (i.e., expanding the field operators  $\Psi(\hat{x})$  and  $\Psi^\dagger(\hat{x}')$  using only the lowest band Wannier functions), these are related to the regime of validity of the Gaussian approximation, when the Wannier functions can be approximated with Gaussian functions. In the Gaussian approximation one finds  $|J_1/J_n| = \exp\left[(n^2 - 1)\frac{\pi^2}{4y}\right] \gg 1$ , also indicating validity of the tight-binding approximation in this regime. Figure 6(a) displays the difference  $\Delta - \Delta_{TBA}$  between the width  $\Delta$  of the first Bloch band, obtained from diagonalization of the single-particle Hamiltonian in Eq. (7), and the width  $\Delta_{TBA}$  evaluated with the tight-binding approximation,

as a function of  $y^{-1}$ . Figure 6(b) displays the difference between the coupling parameters obtained by using the Wannier functions and the modified Gaussian functions as a function of  $y^{-1} < 1$ . We note that for values  $y^{-1} < 1$  the validity of both the tight binding and Gaussian approximation visibly breaks down. This has also been verified by recalculating some of the above phase diagram using the Wannier functions.

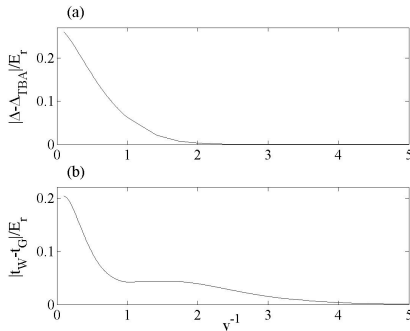


FIG. 6: The upper plot shows the difference  $\Delta - \Delta_{TBA}$ , in units of  $E_R$ , as a function of  $y^{-1}$ , where  $\Delta$  is the width of the first energy band and  $\Delta_W = 2t_W$ , where  $t_W$  is the coupling element obtained from the corresponding Wannier functions in the tight-binding approximation. The lower plot displays  $t_W - t_G$  as a function of  $y^{-1}$ , where  $t_G$  is the coupling element given by the Gaussian approximation.

## V. CONCLUSIONS

We have shown that ultracold bosonic atoms inside a resonator may form stable insulator-like states, and thus enter the Mott phase, which is sustained by and sustains the cavity potential. The dynamics is generally given by the competition between the quantum electrodynamic effects and the quantum fluctuations of the atomic matter waves, which give a non-trivial dependence of the regions of stability and of the collective atomic state on the system parameters. Since the cavity potential depends on the state of the atoms, the behavior differs hence significantly from the one which is studied in open space, where the atomic gas exhibits crossover between a Mott phase and a superfluid state. We have derived the Bose-Hubbard model for this system, whose coefficients depend on the number of atoms. We have determined regions of parameters where the atomic insulator states are stable, predicting the existence of overlapping stability regions for competing Mott states. Bistable behavior is encountered in the vicinity of the shifted cavity resonance, controlled by the pump parameters.

Our theory allows us to determine the state of the atoms when the number is fixed, while in the grand-canonical ensemble no definite prediction on the atomic state can be made. In general, the system will choose the state of minimum energy. This will be also valid when an

external inhomogeneous potential is additionally applied to the atoms. However, it is not clear how the presence of an inhomogeneous potential will modify the insulator-like states, since the state of the system depends in a nontrivial way on global parameters, which determine the local density of the atoms and the intracavity field. The condition that atoms may affect locally the potential, hence giving rise to phonon-like dynamics, may be reached by considering multi-mode resonators, allowing for localized polaritonic excitations. Further novel features are expected, when fermions are considered instead of bosons. These questions will be tackled in future works.

## Acknowledgments

We thank E. Demler, Ch. Maschler, C. Menotti, H. Monien, E. Polzik, J. Reichel, and H. Ritsch for discussions. We acknowledge support from the Swedish government/Vetenskapsrådet, the German DFG (SFB 407, SPP 1116), from the European Commission (EMALI, MRTN-CT-2006-035369; SCALA, Contract No. 015714), from ESF PESC QUDEDIS, and the Spanish Ministry for Education MEC (FIS 2005-04627; QLIQS, FIS2005-08257; Ramon-y-Cajal individual fellowship; Consolider Ingenio 2010 "QOIT").

## APPENDIX A: DERIVATION OF THE EFFECTIVE HAMILTONIAN

We consider Eq. (24), and rewrite it as

$$\dot{b}_\ell = \frac{1}{i\hbar} [b_\ell, \mathcal{H}_0] - iC, \quad (\text{A1})$$

where  $C$  is defined in Eq. (26) and  $\hat{Y} = J_0\hat{N} + J_1\hat{B}$ . We aim at finding an effective Hamiltonian  $\mathcal{H}_{BH}$  of the Bose-Hubbard form, such that

$$C = [b_\ell, \mathcal{H}_{BH}]/\hbar$$

in some thermodynamic limit to be identified.

We expand now operator  $C$  at first order in  $J_1$ , assuming  $J_1 \ll J_0$ , as it is verified in the Mott-insulator state, using  $[\hat{N}, \hat{B}] = 0$  and

$$F(J_0\hat{N} + J_1\hat{B}) \approx F(J_0\hat{N}) + J_1\hat{B}F'(J_0\hat{N}), \quad (\text{A2})$$

where we have introduced the notation

$$F'(J_0\hat{N}) = \left. \frac{\partial}{\partial y} F(y) \right|_{y=J_0\hat{N}}. \quad (\text{A3})$$

At first order in  $J_1$ , we find

$$\begin{aligned} C = & U_0\eta^2 F^\dagger(J_0\hat{N}) [J_0 b_\ell + J_1(b_{\ell+1} + b_{\ell-1})] F(J_0\hat{N}) \\ & + U_0\eta^2 F^\dagger(J_0\hat{N}) J_1 B J_0 b_\ell F(J_0\hat{N}) \\ & + U_0\eta^2 F^\dagger(J_0\hat{N}) J_0 b_\ell J_1 B F'(J_0\hat{N}) + \mathcal{O}(J_1^2). \end{aligned}$$

Let us now consider the commutation relations between the various operators entering this expression. We note that

$$\begin{aligned} [b_\ell, F(J_0\hat{N})] &= (F(J_0(\hat{N}+1)) - F(J_0\hat{N}))b_\ell \\ &= F'(J_0\hat{N})J_0b_\ell + O(1/N^2) \end{aligned} \quad (\text{A4})$$

and it is hence of order  $1/N$ . Similarly, the commutator  $[b_\ell, B] = b_{\ell+1} + b_{\ell-1}$  is at higher order in the expansion in  $1/N$ . Henceforth, we can rewrite

$$\begin{aligned} C &= U_0\eta^2 F^\dagger(J_0\hat{N}) [J_0b_\ell + J_1(b_{\ell+1} + b_{\ell-1})] F(J_0\hat{N}) \\ &\quad + U_0\eta^2 F^\dagger(J_0\hat{N}) J_0b_\ell J_1 B F(J_0\hat{N}) \\ &\quad + U_0\eta^2 F^\dagger(J_0\hat{N}) J_1 B J_0 b_\ell F'(J_0\hat{N}) \\ &\equiv [b_\ell, \mathcal{H}_{BH}], \end{aligned}$$

where

$$\mathcal{H}_{BH} = \hbar\eta^2 U_0 J_1 F^\dagger(J_0\hat{N}) B F(J_0\hat{N}) + G(J_0\hat{N}) \quad (\text{A5})$$

and operator  $G(J_0\hat{N})$  has to be determined from the equation

$$[b_\ell, G(J_0\hat{N})] + U_0\eta^2 F^\dagger(J_0\hat{N}) J_0 b_\ell F(J_0\hat{N}) = 0, \quad (\text{A6})$$

which is valid at the considered order in the expansion in  $1/N$ . At leading order in  $1/N$ , Eq. (A6) is a differential equation, such that  $G'(J_0\hat{N}) = -U_0\eta^2 F^\dagger(J_0\hat{N}) F(J_0\hat{N})$ . Using the explicit form of operator  $F(x)$ , Eq. (30), we find

$$G'(x) = -U_0\eta^2 / (\kappa^2 + (\Delta_c - U_0x)^2)$$

which gives

$$G(x) = \frac{\eta^2}{\kappa} \arctan\left(\frac{\Delta_c - U_0x}{\kappa}\right) \quad (\text{A7})$$

and finally the effective Hamiltonian in Eq. (31).

## APPENDIX B: PERTURBATIVE DERIVATION OF THE ZONE BOUNDARIES

We consider Hamiltonian

$$H = -\tilde{t}(\hat{N})\hat{B} + \frac{U(\hat{N})}{2} \sum_{i=1}^K \hat{n}_i(\hat{n}_i - 1) - \tilde{\mu}\hat{N}, \quad (\text{B1})$$

as given in Eq. (35). This Hamiltonian differs from the standard Bose-Hubbard Hamiltonian, as the coefficients depend on the operator  $\hat{N}$ . We apply now to Eq. (B1) the method of Ref. [32], which allows to determine the region of stability of the Mott-insulator states. The method consists in a perturbative expansion in the parameter  $\tilde{t}$ , which is assumed to be small within the parameter regime of interest. In this limit, for large onsite interaction strength  $U$  (*hard core limit*), in the optical lattice

the configuration which is energetically favorable has the smallest number of atoms per site. For a lattice of  $K$  sites and  $N = Kn_0 + j$  atoms, with  $j < K$ , there will be either  $n_0$  or  $n_0 + 1$  atoms per site. Clearly, when  $N = Kn_0$  atoms ( $j = 0$ ), there exists only one possible ground-state, while for  $N > Kn_0$  several ground state configurations exists, and one has to apply degenerate perturbation theory.

The ground-state of Hamiltonian (B1) is found after imposing periodic boundary conditions, and diagonalizing operator  $\hat{B}$  in the momentum representation. At  $t = 0$  the ground-state for  $N = Kn_0$  is given by

$$|\Psi_0(n_0)\rangle = |n_0, n_0, \dots, n_0\rangle, \quad (\text{B2})$$

corresponding to  $n_0$  atoms per site, while for  $N = Kn_0 + j$ , with  $j > 0$ , they are defined by the relation

$$|\Psi_j(n_0)\rangle = \hat{A}_{k_j}^\dagger |\Psi_{j-1}(n_0)\rangle, \quad (\text{B3})$$

where

$$\hat{A}_{k_j}^\dagger = \frac{1}{\sqrt{K}} \sum_{n=1}^K e^{ink_j a} \frac{\hat{b}_n^\dagger}{\sqrt{\hat{n}_n + 1}} \quad (\text{B4})$$

creates one particle in a site starting from the lowest energy states. Here,  $a = \pi/k$  is the distance between neighboring sites, and the wave vector  $k_j = 2\pi j/Ka$ , with  $j = -\frac{K}{2}, -\frac{K}{2} + 1, \dots, \frac{K}{2} - 1$  (assuming  $K$  even for simplicity). In the position representation, the ground-state Eq.(B2) reads

$$|\Psi_M(n_0)\rangle = |\Psi_0(n_0)\rangle, \quad (\text{B5})$$

while Eqs. (B3), for  $j = \pm 1$ , take the form

$$|\Psi_+(n_0)\rangle = (K(n_0 + 1))^{-\frac{1}{2}} \sum_{n=1}^K \hat{b}_n^\dagger |\Psi_M(n_0)\rangle, \quad (\text{B6})$$

$$|\Psi_-(n_0)\rangle = (K(n_0 + 1))^{-\frac{1}{2}} \sum_{n=1}^K \hat{b}_n |\Psi_M(n_0)\rangle. \quad (\text{B7})$$

The ground state energy is calculated applying perturbation theory in third-order in  $\tilde{t}$  to this unperturbed basis. Due to symmetry, only zeroth and second-order in the perturbation of  $t(\hat{N})\hat{B}$  contribute to the ground-state energies of the Mott-insulator state. For  $N = Kn_0$  one finds

$$\begin{aligned} E_M(n_0) &= \frac{U_{(2)}}{2} K n_0 (n_0 - 1) - \mu_{(2)} K n_0 \\ &\quad - \frac{t_{(2)}^2}{U_{(2)}} 2K n_0 (n_0 + 1) \end{aligned} \quad (\text{B8})$$

while the SF energies for the added particle/hole energies

are

$$\begin{aligned}
E_+(n_0) &= \frac{U_{(1)}}{2} [Kn_0(n_0 - 1) + 2n_0] - \mu_{(1)}(Kn_0 + 1) \\
&\quad - t_{(1)}2(n_0 + 1) - \frac{t_{(1)}^2}{U_{(1)}} [2Kn_0(n_0 + 1) - n_0^2] \\
&\quad + \frac{t_{(1)}^3}{U_{(1)}^2} n_0(n_0 + 1)(n_0 + 2), \\
E_-(n_0) &= -\mu_{(3)}(Kn_0 - 1) + \frac{U_{(3)}}{2} [Kn_0(n_0 + 1) - n_0 + 1] \\
&\quad - t_{(3)}2n_0 - \frac{t_{(3)}^2}{U_{(3)}} [2Kn_0(n_0 + 1) - (n_0 + 1)^2] \\
&\quad - \frac{t_{(3)}^3}{U_{(3)}^2} n_0(n_0 + 1)(n_0 - 1).
\end{aligned} \tag{B9}$$

Here we have used the subscript ( $i$ ) corresponding to the three different cases,  $N = Kn_0$  and  $N = Kn_0 \pm 1$ , see Sec. IV. The limit of stability of the Mott-insulator state is found when the states  $|\Psi_M(n_0)\rangle$  and  $|\Psi_{\pm}(n_0)\rangle$  are degenerate. The conditions  $E_M(n_0) - E_+(n_0) = 0$  and  $E_M(n_0) - E_-(n_0) = 0$  determine the boundaries of the Mott states in the phase diagram  $\tilde{\mu} - \tilde{t} \mu_{\pm}(n_0)$ , thus obtaining the results in Eqs. (50).

- 
- [1] D. Walls, and G. J. Milburn, *Quantum Optics*, (Springer verlag Berlin, 1994).
- [2] *Cavity Quantum Electrodynamics, Advances in Atomic, Molecular and Optical Physics, Supplement 2*, edited by P. R. Berman, (New York: Academic Pres, 1994); S. M. Dutra, *Cavity Quantum Electrodynamics*, (Wiley-Interscience, 2004).
- [3] R. Bonifacio and L. A. Lugiato, Phys. Rev. Lett. **40**, 1023 (1978); Phys. Rev. A **18**, 1129 (1978); Lett. Nuovo Cimento **21**, 505 (1978).
- [4] M. Weidinger, B. T. H. Varcoe, R. Heerlein, H. Walther, Phys. Rev. Lett. **82**, 3796 (1999); B. T. H. Varcoe, S. Brattke, M. Weidinger, H. Walther, Nature **403**, 743 (2000).
- [5] S. Haroche, and J. M. Raimond, *Exploring the Quantum*, (Oxford University Press, 2006).
- [6] W. P. Schleich, *Quantum Optics in Phase Space*, (Wiley, 2001).
- [7] C. J. Hood, T. W. Lynn, A. C. Doherty, A. S. Parkins, and H. J. Kimble, Science **287**, 1447 (2000). P. W. H. Pinkse, T. Fisher, P. Maunz, and G. Rempe, Nature **404**, 365 (2000).
- [8] P. W. H. Pinkse, T. Fisher, P. Maunz, and G. Rempe, Nature **404**, 365 (2000).
- [9] P. Grangier, G. Reymond, and N. Schlosser, Fortsch. Physik Prog. Phys. **48** 859 (2000).
- [10] A.T. Black, H.W. Chan, and V. Vuletić, Phys. Rev. Lett. **91**, 203001 (2003).
- [11] P. Domokos and H. Ritsch, Phys. Rev. Lett. **89**, 253003 (2002)
- [12] J.K. Asbóth, P. Domokos, H. Ritsch and A. Vukics, Phys. Rev. A **72**, 053417 (2005).
- [13] S. Zippilli, G. Morigi, H. Ritsch, Phys. Rev. Lett. **93**, 123002 (2004); Eur. Phys. J. D **31**, 507 (2004); S. Zippilli, J. Asbóth, G. Morigi, H. Ritsch, Appl. Phys. B: Lasers Opt. **79**, 969 (2004).
- [14] S. Slama, C. von Cube, M. Kohler, C. Zimmermann, and Ph. W. Courteille, Phys. Rev. Lett. **94**, 193901 (2005).
- [15] P. Treutlein, D. Hunger, S. Camerer, T. W. Hnsch, and J. Reichel, Phys. Rev. Lett. **99**, 140403 (2007); Y. Colombe, T. Steinmetz, G. Dubois, F. Linke, D. Hunger, and J. Reichel, arXiv:0706.1390.
- [16] S. Slama, G. Krenz, S. Bux, C. Zimmermann, and P.W. Courteille, Phys. Rev. A **75** 063620 (2007).
- [17] I. B. Mekhov, C. Maschler, and H. Ritsch, Phys. Rev. Lett. **98**, 100402 (2007).
- [18] I. B. Mekhov, C. Maschler, and H. Ritsch, arXiv:quant-ph/0702193.
- [19] A. Öttl, S. Ritter, M. Köhl, and T. Esslinger Phys. Rev. Lett. **95**, 090404 (2005); Rev. Sci. Instr. **77**, 063118 (2006).
- [20] I. B. Mekhov, C. Maschler, and H. Ritsch, Nature Phys. **3**, 319 (2007).
- [21] I. Bloch and M. Greiner, Adv. At. Molec. Opt. Phys. **52**, 1 (2005).
- [22] M. Lewenstein *et al.*, cond-mat/0606771.
- [23] D. Jaksch and P. Zoller, Ann. Phys. (N.Y.) **315**, 52 (2005).
- [24] M.P.A. Fisher, P.B. Weichman, G. Grinstein, and D.S. Fisher, Phys. Rev. B **40**, 546 (1989).
- [25] S. Sachdev, *Quantum Phase Transitions* (Cambridge University Press, Cambridge, 1999).
- [26] D. Jaksch, C. Bruder, J.I. Cirac, C.W. Gardiner, and P. Zoller, Phys. Rev. Lett. **81**, 3108 (1998).
- [27] M. Greiner, O. Mandel, T. Esslinger, T. W. Hsch and I. Bloch, Nature **415**, 39 (2002).
- [28] J. Larson, B. Damski, G. Morigi, and M. Lewenstein, arXiv:cond-mat/0608335.
- [29] C. Maschler and H. Ritsch, Phys. Rev. Lett. **95**, 260401 (2005).
- [30] J. K. Asboth, H. Ritsch, and P. Domokos, Phys. Rev. Lett. **98**, 203008 (2007); A. Vukics, C. Maschler, and H. Ritsch, arXiv:quant-ph/0703221.
- [31] N. W. Ascroft, and N. D. Mermin, *Solid State Physics*, (Harcourt Collage Publishers, 1976).
- [32] J.K. Freericks and H. Monien, Europhys. Lett. **26**, 545 (1994); Phys. Rev. B **53**, 2691 (1996).
- [33] The scaling  $U_0 \sim 1/N$  is also found by increasing the cavity length as  $\sqrt{N}$ . This condition also implies, however, that the free spectral range vanishes. The corresponding dynamics then become the one of atomic dipoles interacting strongly with a continuum of modes. In this specific

limit the Jaynes-Cummings model, at the basis of our derivation, is not valid.

- [34] G.G. Batrouni, V. Rousseau, R.T. Scalettar, M. Rigol, A. Muramatsu, P.J.H. Denteneer, and M. Troyer, Phys. Rev. Lett. **89**, 117203 (2002); G.G. Batrouni, F.F. Assaad, R.T. Scalettar, and P.J.H. Denteneer, Phys. Rev. A **72**, 031601(R) (2005).
- [35] D. M. Stamper-Kurn, H.-J. Miesner, A. P. Chikkatur, S. Inouye, J. Stenger, and W. Ketterle, Phys. Rev. Lett. **81**, 2194 (1998); A. J. Daley, P. O. Fedichev, and P. Zoller, Phys. Rev. A **69**, 022306 (2004); A. Griessner, A. J. Daley, S. R. Clark, D. Jaksch, and P. Zoller, Phys. Rev. Lett. **97**, 220403 (2006); A. Griessner, A. J. Daley, S. R. Clark, D. Jaksch, and P. Zoller, New. J. Phys. **9**, 44 (2007).
- [36] T. Vekua, D.C. Cabra, A. Dobry, C. Gazza, and D. Poilblanc, Phys. Rev. Lett. **96**, 117205 (2006), and references therein.
- [37] In the opposite limit of small pumping we also have  $\tilde{t} \rightarrow 0$ , which, however, is within the regime where the Gaussian and the tight-binding approximations are not valid